A diagnostic study of subgrid-scale activation

Hongli Jiang and William R. Cotton

Department of Atmospheric Science, Colorado State University, Fort Collins, Colorado, USA

Received 20 December 2004; revised 30 March 2005; accepted 1 June 2005; published 24 August 2005.

[1] Using large-eddy simulations (LESs) of six observed boundary layer cases as benchmark data sets, we diagnosed vertical velocity as the sum of the grid-mean ($\overline{w}$) and the subgrid-scale w using an empirical method we have developed. We have found that the subgrid-scale w is best characterized by the root-mean square of w'^2. The vertical velocity is expressed in the form of $w = \overline{w} + c\sqrt{\overline{w'^2}}$, where c is diagnosed from LES data to be 0.24. The w is then used to diagnose the cloud droplet numbers using a simple predictive equation of cloud nucleation following previous works in the literature. Good agreement is found between diagnosed cloud droplet concentrations and predicted cloud droplet concentrations using an LES model.

Citation: Jiang, H., and W. R. Cotton (2005), A diagnostic study of subgrid-scale activation, *J. Geophys. Res.*, *110*, D16107, doi:10.1029/2004JD005722.

1. Introduction

[2] There are several approaches to interface cloud microphysics in large-scale models to study aerosol–cloud drop interactions. One is to directly predict the concentrations of cloud droplets in a general circulation model (GCM) [e.g., *Ghan et al.*, 1997; *Lohmann et al.*, 1999]. The limitation of this approach is that the grid-mean vertical velocity in a GCM is much less than that cloud-scale vertical velocities. A second approach is to couple three-dimensional turbulence models to explicit representations of cloud microphysics [*Kogan et al.*, 1994, 1995; *Stevens*, 1996] or to couple a higher-order closure model to explicit representations of cloud microphysics [e.g., *Wang and Wang*, 1994] and to a bulk microphysics [e.g., *Chen and Cotton*, 1983]. The higher-order closure model can have as many as 50 prognostic equations for the mean quantities and higher-order moments, and is computationally too expensive to be used in regional or general circulation or climate forecast models. This approach is taken mostly for studying stratocumulus clouds because of their high frequency of occurrence, large area coverage, and large impact on the Earth radiation budgets. A subset group among the higher-order closure models is coupling the microphysical, turbulent, and radiative modules in a one-dimensional (1-D) model [*Ackerman et al.*, 1995] or a two-dimensional (2-D) model [*Bott et al.*, 1996]. The model of *Ackerman et al.* [1995], however, does not predict vertical velocity, and supersaturations are determined by diffusion only [*Stevens et al.*, 1998]. *Stevens et al.* [1998] suggested that the key to building a physically based 1-D model is to explicitly represent the subgrid-scale turbulent structure and inhomogeneity, its interaction with microphysical processes such as activation of cloud condensation nuclei (CCN), sedimentation of hydrometeors and collection. If the above limitations can be rectified, the shorter integration time makes the use of the 1-D model advantageous over other approaches.

[3] A 1-D (single-column) probability distribution function (PDF) based boundary layer parameterization (hereafter referred to as PDF model) has been recently developed [*Golaz et al.*, 2002a, 2002b]. The PDF model is a higher-order closure model with a closure based on an assumed double Gaussian family of PDFs. It can accurately represent a variety of nonprecipitating boundary layer regimes without arbitrary adjustment of coefficients or parameters. In the PDF model, the subgrid-scale, higher-order vertical velocity moments such as $\overline{w'^2}$ and $\overline{w'^3}$ are predicted, while cloud fraction is diagnosed. These velocity scales provide information that can be used to diagnose subgrid-scale variations of supersaturation. The capability of predicting subgrid-scale variability of higher-order moments and cloud fraction of the PDF model makes it differ from most of the 1-D models. As most single-column and global models drive microphysics with grid box mean supersaturation, they are limited in their ability to represent the physical process of aerosol activation and droplet growth in turbulent updrafts and downdrafts as discussed by *Stevens et al.* [1998].

[4] In this paper the PDF model is extended to include precipitation processes. Here we solve the subgrid-scale supersaturation calculation problem. Our guiding principle in this work is to develop parameterizations of subgrid-scale effects on nucleation, condensation, collection, and precipitation formation without adding a large number of prognostic variables. Previous studies [e.g., *Ghan et al.*, 1993, 1997; *Chuang and Penner*, 1995; *Chuang et al.*, 1997; *Lohmann et al.*, 1999] have used the following expression to represent the predicted cloud droplet number due to activation

$$N_d = \frac{wN_a}{w + \alpha N_a}, \tag{1}$$

where N_a is the total aerosol number concentration, w is the vertical velocity, and α depends on aerosol properties and

0148-0227/05/2004JD005722$09.00

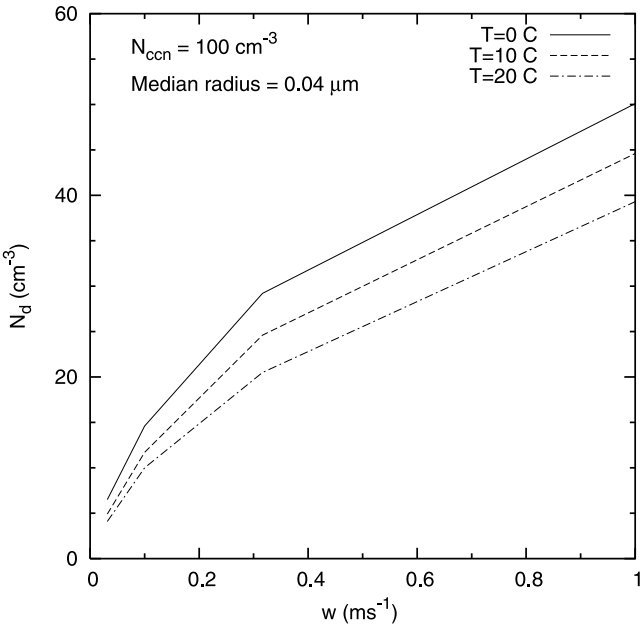

Figure 1. Droplet number activated from RAMS activation scheme.

vertical velocity. The equation used to determine α values will be discussed in section 4. We seek similar simplified approaches to parameterize activation of CCN. We will use large-eddy simulations (LES) of a number of observed boundary layer cases as benchmark data sets to aid in representing subgrid-scale w and to diagnose the cloud droplet concentrations due to activation given in equation (1).

[5] The Regional Atmospheric Modeling System (RAMS) is used to run 3-D LES to generate a synthetic data set. A brief description of the RAMS feature pertinent to this study is given in section 2. The strategy to derive the subgrid-scale w will be presented in section 3. Results from diagnostic analysis of the LES data and conclusions are given in sections 4 and 5.

2. RAMS Activation Scheme

[6] The LES version of RAMS has been used to simulate a wide range of boundary layer cloud systems from Arctic [*Jiang et al.*, 2001] to marine boundary layers [*Jiang et al.*, 2002].

[7] The newest version of bulk microphysics in RAMS is designed to emulate a bin-resolving microphysics model including prediction of cloud droplet number from a fully prognosed CCN field [*Cotton et al.*, 2003; *Saleeby and Cotton*, 2004]. The number of CCN that activate are a function of air temperature, Lagrangian supersaturation production rate (related to vertical velocity and other factors), number concentration of CCN, and median radius of the CCN distribution. Other factors such as CCN chemistry, mean radius, and spectral width are considered fixed for a given simulation since these produce the least relative variability. On the basis of the above CCN characteristics and environmental factors, the fraction of CCN that nucleate into cloud droplets is accessed in RAMS from a lookup table that was previously generated from a detailed bin parcel model [*Saleeby and Cotton*, 2004].

[8] The lookup tables are essentially data tables with four-dimensional arrays containing percentage values of CCN that activate and grow to cloud droplet sizes. The table values vary with air temperature, vertical velocity, CCN concentration, and median radius of CCN distribution. Figure 1 displays droplet concentrations activated as a function of vertical velocity at a selected median radius and CCN concentration over three different air temperatures.

3. Subgrid-Scale Vertical Velocity

[9] Cloud base vertical velocity is an important factor in the cloud drop activation process, and is subject to subgrid-scale variabilities. *Lohmann et al.* [1999] have found that twice as many droplets were activated when the value of w (assuming constant vertical profiles) increased from 0.1 m s^{-1} to 1 m s^{-1} while other conditions were held constant in equation (1) in their sensitivity study. They prescribed the subgrid-scale vertical velocity for the entire grid cell as $w = \overline{w} + c\sqrt{\mathrm{TKE}}$, where $\overline{w}$ is the grid-mean vertical velocity, TKE is turbulent kinetic energy predicted by a higher-order closure model, and c is set to be 0.7.

[10] In this study, we preform diagnostic analyses of LES data to seek appropriate vertical velocity scales that can be derived from higher-order closure models for use in predicting droplet activation. The detailed procedure is described in the following.

[11] Six cases used by the Global Energy and Water Experiment (GEWEX) Cloud Study System (GCSS) working grouping I, the boundary layer cloud intercomparison working group have been selected. They range from trade wind cumulus (BOMEX) [*Siebesma et al.*, 2003], cumulus over land (ARM) [*Brown et al.*, 2002], Stratocumulus (ASTEX, FIRE, DYCOMS II) [*Bretherton et al.*, 1999; *Moeng et al.*, 1996; *Stevens et al.*, 2005], and trade wind cumulus under a strong inversion (ATEX) [*Stevens et al.*, 2001]. The stratocumulus cases exhibit cloud fractions (defined as fraction of grid columns has cloud liquid water content greater than 1×10^{-6} kg kg^{-1}) close to 1, the two cumuli have cloud fractions from 0.05 (BOMEX) to 0.1 (ARM), and ATEX has a cloud fraction about 0.5.

[12] RAMS is set up exactly as described in those intercomparison cases. For the cases we participated in the intercomparison, the results obtained with RAMS compared well with other LES models and observations when available. All cases are simulated on a three dimensional (3-D) domain. Simulations are typically done on a domain of 64 $\times$ 64 with a 100 m grid spacing in the horizontal and 30 m grid spacing in the vertical with the number of vertical grid points dependent on the specific cases. The domain is thus 6400 m by 6400 m in the horizontal, and 1500 to 4000 m in the vertical. A time step of 2 s is used in all integrations.

[13] Using the bulk microphysics with its CCN activation parameterization in RAMS, large-eddy simulations of the six observed boundary layer cases are performed with an initially uniform CCN concentrations of 100 cm^{-3} for all the cases. In the LES various clouds activate the CCN to form cloud droplets with a concentration N_d. The simulated cloud layer is sampled every 5 min from the LES outputs to

Table 1. Values of $\overline{N_d}$, $\sqrt{\overline{w'^2}}$, and w Derived From LES

Experiment	$\overline{N_d}$, cm^{-3}	$\sqrt{\overline{w'^2}}$, m s^{-1}	w, m s^{-1}	c[a]
ARM	5.8	0.402	0.05	0.124
ASTEX	11.1	0.201	0.11	0.547
ATEX	5.8	0.314	0.05	0.159
BOMEX	4.3	0.335	0.035	0.104
DYCOMS II	12.1	0.406	0.13	0.320
FIRE	9.5	0.425	0.08	0.188

[a] c is defined through w = $c\sqrt{\overline{w'^2}}$; see text for details.

obtain an average droplet concentration $\overline{N_d}$. Given the CCN spectra and the computed average $\overline{N_d}$ we can identify the w scale that has yielded a $\overline{N_d}$ for the pressure and temperature at the sample level from the activation scheme (see Figure 1). From the PDF of w derived from the LES data, we determine whether there exists a w moment corresponding to the w that yielded $\overline{N_d}$. Our approach is to repeatedly sample the LES data for all six cases to evaluate the appropriate w scale.

[14] We have found the characteristic w moment that best described the diagnosed activated cloud droplet concentrations is the square root of $\overline{w'^2}$. Table 1 lists values of mean droplet number ($\overline{N_d}$) predicted by the RAMS activation scheme, $\sqrt{\overline{w'^2}}$, where $w' = w - \overline{w}$ and $\overline{w}$ is a grid mean, and the w identified from N_d and w relationship (Figure 1) when other parameters in the RAMS activation scheme are held constant for all six cases. The overbars in both $\overline{N_d}$ and $\overline{w'^2}$ denote averaged quantities. The computed $\overline{N_d}$ and $\overline{w'^2}$ are horizontally averaged over the x-y plane (grid mean), and vertically averaged over the cloud layer. The modeled N_d is approximately constant with height in the cloud region consistent with what is observed in the Arctic [*Curry*, 1986] and in the marine boundary layer [*Duynkerke et al.*, 1995]. Averaging over the cloud layer creates a constant N_d profile in the cloud layer similar to observed. $\overline{w'^2}$ is similarly averaged as N_d to be consistent and for simplicity purpose. The parameter c is determined by assuming $w = c\sqrt{\overline{w'^2}}$. As shown in Table 1, c varies from smaller values for cumulus clouds (ARM, BOMEX) to two to four times larger for Stratocumulus clouds (ASTEX, DYCOMS II) with an median value of 0.24 averaged among all six cases. This value is much smaller than that used by *Lohmann et al.* [1999]. The vertical velocity used throughout this study is the sum of the grid-mean ($\overline{w}$) and a subgrid-scale vertical velocity as $w = \overline{w} + c\sqrt{\overline{w'^2}}$ with $c = 0.24$. We substitute this w into equation (1) and diagnose the droplet number concentration predicted in equation (1).

[15] It should be pointed out that w defined as above implies that the subgrid-scale velocity is always positive since only the positive solution of the square root is taken into consideration. That is because activation takes place only in upward motions, and thus the negative solution of square root is ignored. Note that the grid-mean $\overline{w}$ (defined as $\frac{1}{N}\sum_{i=1}^{N} w$, where N is the total number of sample points) is usually so small to be meaningless, but it is included here for a complete definition.

4. Cloud Drop Number and α

[16] The parameter α in equation (1) depends on aerosol properties and vertical velocity. Following *Chuang et al.* [1997], their expressions of α_l (over land) and α_o (over ocean) are given below.

$$\text{over land}\quad \alpha_l = 0.04095 + 21.587X_l \tag{2}$$

$$\text{over ocean}\quad \alpha_o = 0.02215 - 0.1329X_o + 3.0737X_o^2 \tag{3}$$

where

$$X_l = (\log w)\left[1 - (\log w)\left(0.5 + \gamma/\beta^4\right)/(\log N_a)^2\right]/(\log N_a)^{5+\gamma/\beta^3} \tag{4}$$

$$X_o = (\log w)\left[1 - (\log w)\left(0.5 + 0.2\gamma/\beta^3\right)/(\log N_a)^2\right] /(\log N_a)^{2+0.1\gamma/\beta^2} \tag{5}$$

[17] Note that equations (2) and (3) are identical to the equations (2a) and (2b), respectively, given by *Chuang et al.* [1997]. The symbols in equations (4) and (5) are slightly different from *Chuang et al.* [1997] to be consistent with all the symbols used in this study. We use a simpler expression for X_l and X_o after dropping the γ terms that are related to the properties of anthropogenic sulfate aerosols. Aerosol particles (initial CCN) are assumed to be ammonium sulfate, and contributions from anthropogenic sulfate aerosols are not considered in this study. For comparison purpose, we tested with α_l and α_o both of which are dependent on vertical velocity w and aerosol concentrations N_a (equations (4) and (5)), and a constant α value of 6.4×10^{-11} m^4 s^{-1} used by *Ghan et al.* [1993] to diagnose cloud droplet number due to activation from LES data. Table 2 lists values of N_d diagnosed using equation (1) for 3 different α. The diagnosed cloud droplet number are also compared directly with droplet number predicted in the LES (second column in Table 2). N_a is 100 cm^{-3} for all the cases to be consistent. Note that this value of N_a is probably low for the case over land.

[18] In the case of the constant α value of 6.4×10^{-11} m^4 s^{-1} labeled as N_d(α-Ghan) in Table 2 (third column), N_d ranges from 53 cm^{-3} to 88 cm^{-3} among the six cases. They indicate that the activation rate is about 53% to 88% by simply calculating the ratio of N_d to N_a. $N_d(\alpha_o)$ is calculated using α_o in equation (1), and the activation rate varies from 16% to 36%. $N_d(\alpha_l)$ is calculated with α_l replacing α in equation (1), and the activation rate ranges

Table 2. Cloud Droplet Number N_d Predicted Using Different α Values

Experiment	N_d(LES), cm^{-3}	N_d(α-Ghan), cm^{-3}	$N_d(\alpha_o)$, cm^{-3}	$N_d(\alpha_l)$, cm^{-3}
ARM	5.8	57.6	24.2 (0.123)[a]	8.3 (0.584)
ASTEX	11.1	84.6	21.5 (0.077)	7.1 (0.444)
ATEX	5.8	67.4	18.6 (0.074)	6.1 (0.377)
BOMEX	4.3	53.2	15.9 (0.090)	5.3 (0.499)
DYCOMS II	12.1	86.6	34.7 (0.132)	12.0 (0.588)
FIRE	9.5	88.5	36.1 (0.136)	12.5 (0.605)

[a] Values in parentheses are the cloud-layer-averaged α values in units of 10^{-8} m^4 s^{-1}.

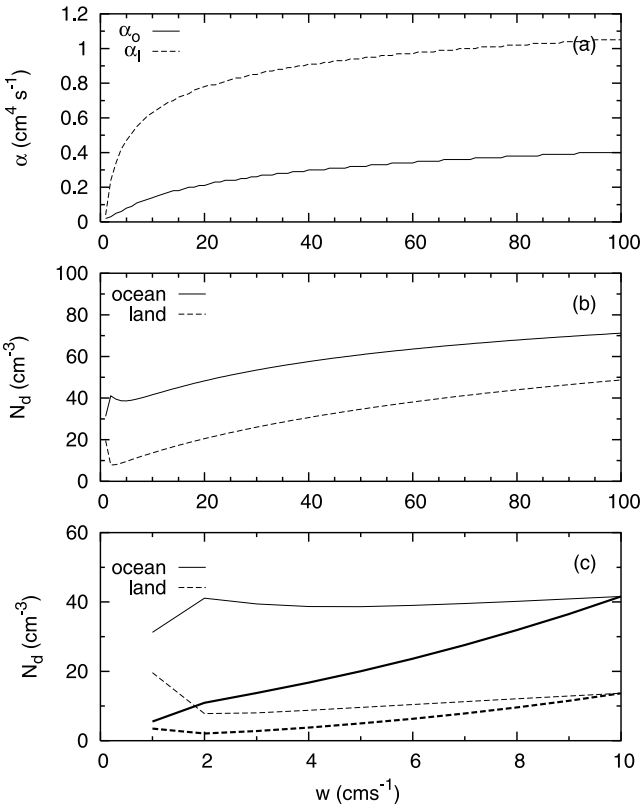

Figure 2. Analytic analysis of (a) α and (b and c) N_d as a function of w. The thicker lines denote N_d after w adjustment for over ocean and land, respectively. See text for details.

from 5.3% to 12.5% for the same N_a. The results of $N_d(\alpha_l)$ are in general agreement with *Lohmann et al.* [1999] who found that the activation rate is about 8% over ocean and 11% over land for the same N_a. The diagnosed $N_d(\alpha_l)$ agrees very well with the predicted N_d using LES data. Comparison among the α values listed in the parentheses in column four and five of Table 2 reveals that α_l is on average 5 times of α_o, while the smallest α_o is 1 order of magnitude larger than the constant value of α-Ghan. These values, however, are all in the range of 1×10^{-12} m^4 s^{-1} to 1×10^{-8} m^4 s^{-1} [*Lohmann et al.*, 1999].

[19] The strong dependence of the predicted cloud droplet number on α, and thus on w when N_a is constant warrants further attention to equations (2) and (3). Analytic results of equations (1), (2), and (3) as a function of w are plotted in Figure 2. The rate of change of α_l with respect to w is the biggest when w is less than 0.1 m s^{-1}, where α_l and α_o separate from each other quickly and the differences between them remain about the same afterward (Figure 2a). The differences in α manifested themselves inversely in N_d (Figure 2b), which is calculated using equation (1) and N_a is 100 cm^{-3}. N_d over the ocean can be as high as 2.5 times that over land (Figure 2b).

[20] *Chuang et al.* [1997] pointed out that the α given in equations (2) and (3) are derived to work for w greater than 0.1 m s^{-1}. They suggested that for w less than 0.1 m s^{-1}, the predicted N_d in equation (1) should be reduced by a factor to $N_d(w) = N_d(w = 0.1 \text{ m s}^{-1})[2 - \log w]^{-2.5}$. The reduction factor $[2 - \log w]^{-2.5}$ varies from 0.177 to 1 as w increases from 0.01 m s^{-1} to 0.1 m s^{-1}. Figure 2c shows the N_d before and after the adjustment with focusing on $w <$ 0.1 m s^{-1}. N_d over ocean jumps to 40 cm^{-3} when w is only 0.02 m s^{-1} (Figure 2c, thin solid line). It is nonphysical, and unrealistic when comparing to the activation scheme shown in Figure 1. After the adjustment, N_d increases more slowly and naturally with w (the thicker lines). For boundary layer clouds, w is often less than 0.1 m^{-1} (Table 1), and the adjustment is necessary in order to use equation (1) to realistically predict the number concentration of droplets due to activation. It should be noted that the N_d values listed in column 4 and 5 of Table 2 have been multiplied by the reduction factor.

5. Concluding Remarks

[21] In an effort to extend the PDF model to include precipitation processes, we first solve the subgrid-scale activation problem. In this study, we have identified an empirical relationship between the higher-order vertical velocity moments (second order, w'^2) and the subgrid-scale vertical velocity (w). The w has been used to diagnose the cloud droplet numbers using a simple predictive equation of cloud nucleation following the work of *Chuang and Penner* [1995], *Chuang et al.* [1997], *Ghan et al.* [1993, 1997], and *Lohmann et al.* [1999]. Comparison between the diagnosed cloud droplet number using equation (1) and the predicted cloud droplet numbers in the RAMS activation scheme using LES data are performed for all six boundary layer cases. The predicted (Table 2, second column) cloud droplet numbers using LES data agree very well with the diagnosed cloud droplet numbers (Table 2, fifth column) when α_l is used in equation (1).

[22] We have shown that the simple parameterization given in equation (1) is sufficient to predict cloud droplet nucleation in a large-scale model given an appropriate estimate of cloud-scale vertical velocities. Equation (1) will be implemented in the PDF model while the higher-order vertical velocity moments and the subgrid-scale vertical velocity (w) predicted in the PDF model will be used in the empirical relationship that we have identified using LES data in this diagnostic study.

[23] To proceed to collection and hydrometeor sedimentation processes, we will not only need to derive parameterizations as simple as equation (1), but to include representation of cloud-scale water contents. For a cumulus population the grid-mean temperature, T, and total water mixing ratio, r_t, are not representative of subgrid cloudy conditions. A new sampling technique has been developed to sample only the saturated portion of the r_t PDF space [*Larson et al.*, 2005]. The method is known as Latin hypercube sampling (LHS), which is a type of Monte Carlo sampling. The LHS involves sampling in an assumed basis function for the family of PDFs. This approach allows us to sample only the cloudy part of the grid box, which will yield saturated values of r_t, θ_l, and w. The sampled saturated values of these variables are then used to drive the collection processes. This approach is very promising but requires a lot of new thinking and development. This will be described in a later paper.

[24] **Acknowledgments.** The comments of two anonymous reviewers greatly improved the clarity of this manuscript. This research was supported by grants from the NSF under grant ATM-0215367.

References

Ackerman, A. S., O. B. Toon, and P. V. Hobbs (1995), A model for particle microphysics, turbulent mixing, and radiative transfer in the stratocumulus-topped marine boundary layer and comparison with measurements, *J. Atmos. Sci.*, *52*, 1204–1236.

Bott, A., T. Trautmann, and W. Zdunkowski (1996), A numerical model of the cloud-topped planetary boundary layer: Radiation, turbulence and spectral microphysics in marine stratus, *Q. J. R. Meteorol. Soc.*, *122*, 635–667.

Bretherton, C. S., S. K. Krueger, M. C. Wyant, P. Bechtold, E. Van Meijgaard, B. Stevens, and J. Teixeira (1999), A GCSS boundary-layer cloud model intercomparison study of the first ASTEX Lagrangian experiment, *Boundary Layer Meteorol.*, *39*, 341–380.

Brown, A. R., et al. (2002), Large-eddy simulation of the diurnal cycle of shallow cumulus convection over land, *Q. J .R. Meteorol. Soc.*, *128*, 1075–1094.

Chen, C., and W. R. Cotton (1983), A one-dimensional simulation of the stratocumulus-capped mixed layer, *Boundary Layer Meteorol.*, *25*, 289–321.

Chuang, C. C., and J. E. Penner (1995), Effects of anthropogenic sulfate on cloud drop nucleation and optical properties, *Tellus, Ser. B*, *47*, 566–577.

Chuang, C. C., J. E. Penner, K. E. Taylor, and A. S. Grossman (1997), An assessment of radiative effects of anthropogenic sulfate, *J. Geophys. Res.*, *102*, 3761–3778.

Cotton, W. R., et al. (2003), RAMS 2001: Current status and future directions, *Meteorol. Atmos. Phys.*, *82*, 5–9, doi:10.1007/s00703-001-0584-9.

Curry, J. A. (1986), Interactions among turbulence, radiation, and microphysics in Arctic stratus clouds, *J. Atmos. Sci.*, *43*, 90–106.

Duynkerke, P. G., H. Q. Zhang, and P. J. Jonker (1995), Microphysical and turbulent structure of nocturnal stratocumulus as observed during ASTEX, *J. Atmos. Sci.*, *52*, 2778–2787.

Ghan, S. J., C. C. Chuang, and J. E. Penner (1993), A parameterization of cloud droplet nucleation. Part I: Single aerosol type, *Atmos. Res.*, *30*, 197–221.

Ghan, S. J., L. R. Leung, and R. C. Easter (1997), Prediction of cloud droplet number in a general circulation model, *J. Geophys. Res.*, *102*, 21,777–21,794.

Golaz, J.-C., V. E. Larson, and W. R. Cotton (2002a), A PDF-based model for boundary layer clouds. Part I: Method and model description, *J. Atmos. Sci.*, *59*, 3540–3551.

Golaz, J.-C., V. E. Larson, and W. R. Cotton (2002b), A PDF-based model for boundary layer clouds. Part II: Model results, *J. Atmos. Sci.*, *59*, 3552–3571.

Jiang, H., G. Feingold, W. R. Cotton, and P. G. Duynkerke (2001), Large-eddy simulations of entrainment of cloud condensation nuclei into the Arctic boundary layer: 18 May 1998 FIRE/SHEBA case study, *J. Geophys. Res.*, *106*, 15,113–15,122.

Jiang, H., G. Feingold, and W. R. Cotton (2002), Simulations of aerosol-cloud dynamical feedbacks resulting from entrainment of aerosol into the marine boundary layer during the Atlantic Stratocumulus Transition Experiment, *J. Geophys. Res.*, *107*(D24), 4813, doi:10.1029/2001JD001502.

Kogan, Y. L., D. K. Lilly, Z. N. Kogan, and V. V. Filyushkin (1994), The effect of CCN regeneration on the evolution of stratocumulus cloud layers, *Atmos. Res.*, *33*, 137–150.

Kogan, Y. L., M. P. Khairoutdinov, D. K. Lilly, Z. N. Kogan, and Q. Liu (1995), Modeling of stratocumulus cloud layers in a large eddy simulation model with explicit microphysics, *J. Atmos. Sci.*, *52*, 2923–2940.

Larson, E. V., J.-C. Golaz, H. Jiang, and W. R. Cotton (2005), Supplying local microphysics parameterization with information about subgrid variability: Latin hypercube sampling, *J. Atmos. Sci.*, in press.

Lohmann, U., J. Feichter, C. C. Chuang, and J. E. Penner (1999), Prediction of the number of cloud droplets in the ECHAM GCM, *J. Geophys. Res.*, *104*, 9169–9198.

Moeng, C.-H., et al. (1996), Simulation of a stratocumulus-topped planetary boundary layer: Intercomparison among different numerical codes, *Bull. Am. Meteorol. Soc.*, *77*, 261–278.

Saleeby, S. M., and W. R. Cotton (2004), A large droplet mode and prognostic number concentration of cloud droplets in the RAMS@CSU model. Part I: Module descriptions and supercell test simulations, *J. Appl. Meteorol.*, *43*, 182–195.

Siebesma, A. P., et al. (2003), A large eddy simulation intercomparison study of shallow cumulus convection, *J. Atmos. Sci.*, *60*, 1201–1219.

Stevens, B. (1996), On the dynamics of precipitating stratocumulus, Ph.D. dissertation, 140 pp., Colo. State Univ., Ft. Collins.

Stevens, B., W. R. Cotton, and G. Feingold (1998), A critique of one- and two-dimensional models of boundary layer clouds with a binned representation of drop microphysics, *Atmos. Res.*, *47–48*, 529–553.

Stevens, B., et al. (2001), Simulations of trade-wind cumuli under a strong inversion, *J. Atmos. Sci.*, *58*, 1870–1891.

Stevens, B., et al. (2005), Evaluation of large-eddy simulations via observations of nocturnal marine stratocumulus, *Mon. Weather Rev.*, *133*, 1443–1462.

Wang, S., and Q. Wang (1994), Roles of drizzle in a one-dimensional third-order turbulence closure model of the nocturnal stratus-topped marine boundary layer, *J. Atmos. Sci.*, *51*, 1559–1576.

W. R. Cotton and H. Jiang, Department of Atmospheric Science, Colorado State University, Fort Collins, CO 80523, USA. (cotton@atmos.colostate.edu; jiang@atmos.colostate.edu)